ISOMAse
International Society of Ocean, Mechanical and Aerospace Scientists and Engineers

Journal of Ocean, Mechanical and Aerospace
-Science and Engineering-
30th November 2024. Vol.68 No.3

November 30, 2024

Study of the Secondary Flow Formed on Two-Channel Junction Using Computational Fluid Dynamics

Tasya Mahardika Pratiwi,[a], Yoga Satria Putra[a,*], Joko Sampurno[a], Muhardi[a], Yuris Sutanto[b]

[a)] *Geophysics Program Study, Faculty of Mathematics and Natural Science, Tanjungpura University, Indonesia*
[b)] *Physics Program Study, Faculty of Mathematics and Natural Science, Tanjungpura University, Indonesia*

*Corresponding author: yogasatriaputra@physics.untan.ac.id

Paper History

Received: 19-September-2024
Received in revised form: 17-September-2024
Accepted: 30-November-2024

ABSTRACT

Information about the secondary flow formed at the junction is crucial for identifying areas vulnerable to erosion. This study aims to build a water flow simulation at a two-channel junction with varying angles using Computational Fluid Dynamics (CFD). The goal of the simulation is to analyze the velocity changes on each variation of angles (90°, 70°, 50°, 30°, and 10°) on the two-channel junction. The validation of these flow patterns is significantly connected to the reference data. The secondary flow is formed as the impact of the velocity changes, and the main channel flow meets the branch channel flow. The flow patterns at the 90° junction exhibit similar formation, as evidenced by secondary zones formed around the junction, such as the contraction and separation zones. The contraction zone forms in areas near junctions with high-velocity values, while the separation zone develops in areas where velocity decreases due to the impact of two flows. This study found that CFD effectively analyses velocity changes on two-channel junctions.

KEYWORDS: *CFD, OpenFOAM, RANS k-Omega, Secondary flow, Two-channel junction*.

NOMENCLATURE

P	Pressure
U	Velocity
t	Time
H	Channel Height
L	Channel Length
θ	Channel Angle
Z	Water Depth
x	Longitudinal Distance x-direction
y	Lateral Distance y-direction
z	Vertical Distance z-direction
u	Velocity in the x-direction
v	Velocity in the y-direction
w	Velocity in the z-direction
Re	Reynolds Number
∇	Divergence Operator
ρ	Fluid Density
Δx	Grid Size, x-component
Δy	Grid Size, y-component
Δz	Grid Size, z-component
CFD	Computational Fluid Dynamics
OpenFOAM	Open Field Operation and Manipulation
RANS	Reynolds-Averaged Navier-Stokes

1.0 INTRODUCTION

Interaction between flow components at channel confluences results in complex phenomena. Phenomena such as velocity changes and the formation of secondary flow zones may occur depending on the direction and velocity of the fluids. Additionally, irregular flow patterns could potentially impact the overall efficiency of the fluid system. Understanding this issue is essential for designing and managing channels efficiently, and it is important to anticipate where and when these zones will develop to identify potential issues such as erosion and sedimentation. Computational Fluid Dynamics (CFD) can analyze secondary flow that may develop at a two-channel junction.

Various researchers have extensively studied the flow phenomena at open channel confluences using different theoretical and numerical methods. Flow in a 90° channel was analyzed numerically using the Computational Fluid Dynamics (CFD) approach [1][5] and SSIIM2.0, a three-dimensional (3D) numerical model [4]. Recent 3D research was conducted using many methods, followed by comparing the methods to evaluate their effectiveness. The numerical comparison between Detached Eddy Simulation (DES) and Reynolds-Average Navier-Stokes (RANS) conducted thus results in DES being significantly more effective in predicting the velocity redistribution in the channel due to non-linear interaction between the main flow and the cross-flow [2]. Along with the bends channel, river confluence has been studied to understand flow transport and sedimentation and provide a good account of information about the morphodynamics of the river junctions

JOMAse | Received: 19-September-2024 | Accepted: 30-November-2024 | [(68) 3: 106-117]
Published by International Society of Ocean, Mechanical and Aerospace Scientists and Engineers, www.isomase.org., ISSN: 2354-7065 & e-ISSN: 2527-6085

[3][9]. The effect of flow and geometrical conditions has been characterized to understand the important factors of the channel bends, such as angle of confluence, width ratio, and bed martial properties [6]. Experimental research was conducted to understand the flow mechanism in open-channel junctions, in addition to analyzing the physical condition of flow between the main channel and the branch channel [7] and the pattern of flow studied numerically, focusing on secondary flow formed due to the impact of two branches near the junction [8].

The CFD has become a crucial tool in scientific research design. This method effectively addresses issues related to fluid flow behavior, such as velocity distribution, flow pressure, and temperature within complex systems [10]. Velocity fluctuation was investigated through an experimental study in hydraulic rough open-channel to identify the effect of aspect ratio. In the outer region, the streamline and vertical turbulence intensities are greater due to the effect of side walls in narrow open channel flow [11]. A three-dimensional flow velocity was used to investigate the streamlines in a 180° sharp bend, and it was found that two-clockwise vortices were formed at the 90° section [12]. Numerical simulations of secondary river bends and river confluence were compared to predict the complex flow field and velocity distribution [13-14], while different mathematical methods were also used in compound open channels to discuss the longitudinal velocity distribution [15]. Observation of the secondary circulation in natural river bend showed the primary flow vertical profile is deformed to a maximum value below the water surface [16].

In addition to analytical approaches, experimental data of confluent channels were used to compare and evaluate the models' numerical result and validity to predict the secondary flow's behavior utilizing standard k-ε and realizable k-ε turbulence. In contrast, both turbulences showed good performance due to the geometry of the channel [17]. Besides that, a numerical simulation and modeling of the secondary flow were also conducted by different turbulence models [18, 19, 20], while a transport modeling of the secondary flow was conducted to observe sedimentation and erosion [21- 22].

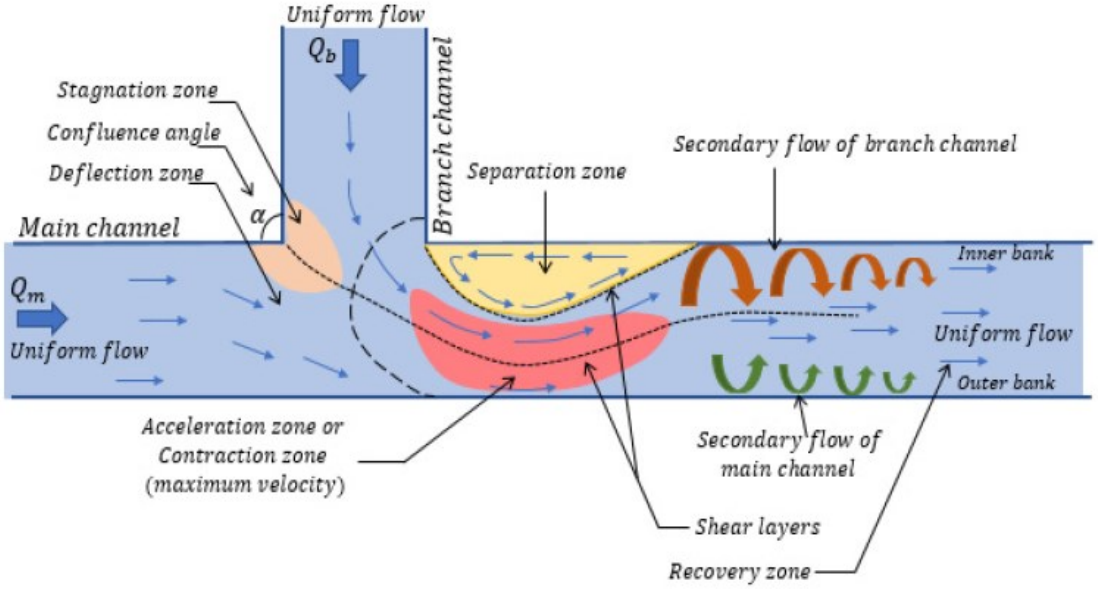

Figure 1: Flow pattern and secondary flow structure in confluent channel [1]

Based on the issues in previous studies, this research will conduct as an investigation of the secondary flow effect in a two-channel junction by analyzing the velocity changes using the Computational Fluid Dynamics (CFD) approach with experimental data by Shumate, Eric Dean (1998) [7]. The simulation utilized the open-source software OpenFOAM and the Reynolds-Averaged Navier-Stokes (RANS) k-Omega turbulence model as the solver. The geometry of the simulation is designed as an open-channel junction, which varies to 5 different angles (90°, 70°, 50°, 30°, and 10°) to investigate the secondary flows that occur in each variation of junction angle. This study aims to improve safety at junctions by addressing transportation challenges and risks. It also seeks to optimize shipping routes, reducing travel time and costs. Additionally, the findings can predict sediment deposition, aiding in better maintenance and environmental management of waterways.

2.0 METHODOLOGY

Numerical methods were used to create a three-dimensional (3D) simulation on the two-channel junction, and open-source OpenFOAM was utilized to create a water flow; the RANS k-Omega was used as the turbulent model. Several stages were conducted, such as a literature review and SALOME 9.11.0, which were used to create a geometry and simulation view domain using ParaView 5.11.2.

2.1 Resource and Equipment

Secondary data were used to study the flow pattern of the 90° channel junction. This data includes experimental and analytical findings from Shumate and Eric Dean (1998) [7]. Research was utilized using hardware and software equipment, as outlined in Table 1.

JOMAse | Received: 19-September-2024 | Accepted: 30-November-2024 | [(68) 3: 106-117]
Published by International Society of Ocean, Mechanical and Aerospace Scientists and Engineers, www.isomase.org., ISSN: 2354-7065 & e-ISSN: 2527-6085

Table 1: Instruments Used in the Study

No	Tools	Specification
1	Laptop	AMD *Ryzen7* 4000 *series* 4800H (2.90 GHz), 16 GB
2	Open-Source OpenFOAM Software	OpenFOAM-dev Version
3	Ubuntu	22.04.3 LTS Version
4	SALOME software	9.11.0 Version
5	ParaView software	5.11.2 Version

2.2 Computational Domain

The geometry model was created using SALOME 9.11.0 software, and the flow simulation of the confluent channel was conducted numerically with the computational domain, as shown in Figure 2(a). The domain of the 90° channel serves as analytical validation to compare against the flow pattern and secondary flow structure in confluent channel junction conducted by Shumate, Eric Dean. (1998) [7], with the length of the main channel and branch channel inlet equal to 2 m, the main channel outlet 7 m, and 0.914 m channel width with a water depth of 0.296 meters. The domain was then created by varying the branching angles. Thus, the angles are 70°, 50°, 30°, and 10°, using the same length and width as the domain of the 90° channel. Five boundaries bound the domain channels: main channel inlet, branch channel inlet, outlet, top, bottom, and walls (Figure 2(b)). Five domain variations facilitated using SALOME 9.11.0 software employed tetrahedral mesh with the Netgen 1D-2D-3D algorithm. Mesh utilizing a "fine" type fineness with a maximum mesh size of 0.04 m and a minimum mesh size of 0.01 m.

Boundary conditions in the computational domain within OpenFOAM were configured in the "system" folder, specifically the "blockMeshDict" file [23]. Physical properties were set with gravity (g) value at 9.8 m/s^2, surface tension (γ) at 0.07 N/m, water density (ρ) at 1.0 x 10^3 kg/m^3 and kinematic viscosity of air (μ) at 1.0 x 10^{-6} m^2/s. Simulation run using Raynods-Average Navier-Stokes (RANS) k-Omega turbulence model, where the boundary conditions were adjusted to an open channel, in which the upper part of the channel filled with air and plotted with a value of zero. Channel flow form was calculated in the Linux Ubuntu 22.04.3 LTS terminal, and visualization was performed using open-source ParaView software 55.11.2 version. The flow condition and dimension values of this simulation are detailed in Table 2.

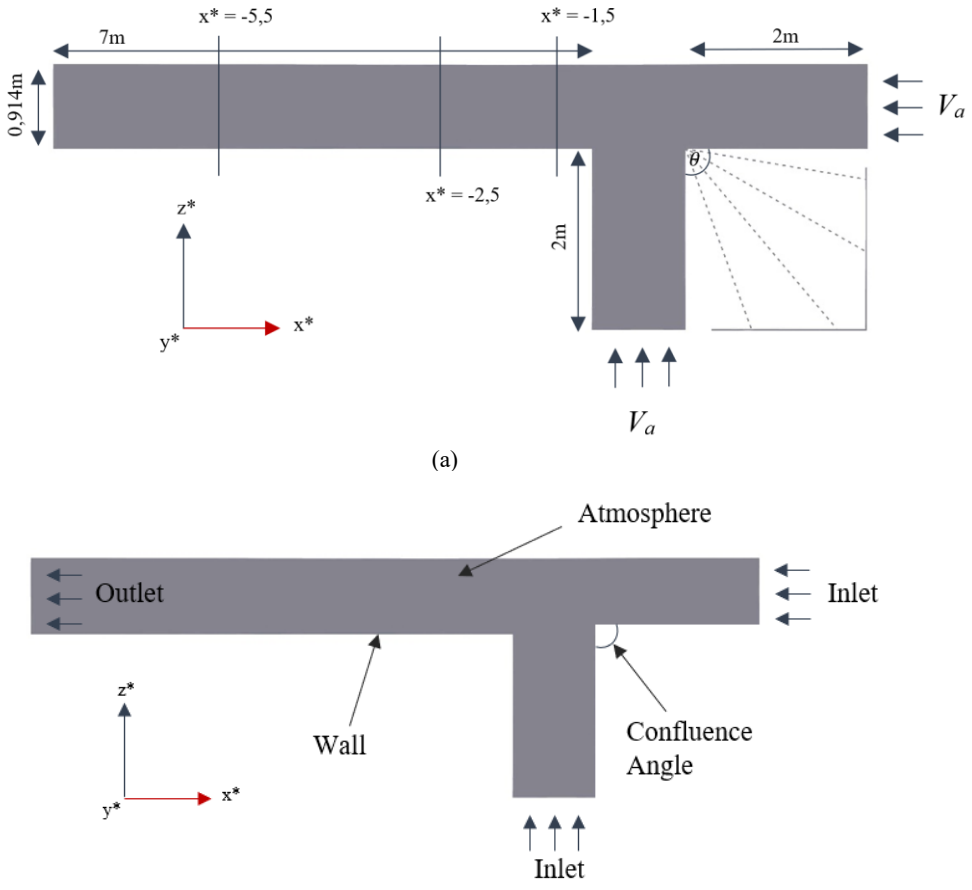

Figure 2: Computational domains: (a) Confluent channel with five variations of junction angle, (b) boundary condition

JOMAse | Received: 19-September-2024 | Accepted: 30-November-2024 | [(68) 3: 106-117]
Published by International Society of Ocean, Mechanical and Aerospace Scientists and Engineers, www.isomase.org., ISSN: 2354-7065 & e-ISSN: 2527-6085

Table 2: Flow condition and dimension values

Variable	Symbol	Value
Downstream water depth	Z	0.296 m
Channel width	L	0.914 m
Velocity	U	0.628 m/s
Channel Angle	θ	90°
		70°
		50°
		30°
		10°

2.3 Flow model

Inter Foam is a computational solver in this simulation. At the same time, the equations are utilized in OpenFOAM, specifically for multiphase cases that apply the Navier-Stokes equations to address problems involving continuity and momentum in fluid and turbulent flows.

$$\nabla . u = 0 \tag{1}$$

where $\nabla . u$ at equation (1) given as velocity divergence in vector u, alternatively can be expressed to equation (2) and (3):

$$div(u) = 0 \tag{2}$$

$$\frac{\partial u_i}{\partial x_i} = 0 \tag{3}$$

while the Navier-Stokes equations used in CFD are written as:

Continuity:

$$\frac{\partial \rho}{\partial t} + \frac{\partial (\rho u)}{\partial x} + \frac{\partial (\rho v)}{\partial y} + \frac{\partial (\rho w)}{\partial z} = 0 \tag{4}$$

Momentum in the x-direction:

$$\frac{\partial (\rho u)}{\partial t} + \frac{\partial (\rho u^2)}{\partial x} + \frac{\partial (\rho uv)}{\partial y} + \frac{\partial (\rho uw)}{\partial z} = -\frac{\partial \rho}{\partial y} + \frac{1}{Re_r}\left(\frac{\partial \tau_{xx}}{\partial x} + \frac{\partial \tau_{xy}}{\partial y} + \frac{\partial \tau_{xz}}{\partial z}\right) \tag{5}$$

Momentum in the y-direction:

$$\frac{\partial (\rho v)}{\partial t} + \frac{\partial (\rho uv)}{\partial x} + \frac{\partial (\rho v^2)}{\partial y} + \frac{\partial (\rho vw)}{\partial z} = -\frac{\partial \rho}{\partial y} + \frac{1}{Re_r}\left(\frac{\partial \tau_{xy}}{\partial x} + \frac{\partial \tau_{yy}}{\partial y} + \frac{\partial \tau_{yz}}{\partial z}\right) \tag{6}$$

Momentum in the z-direction:

$$\frac{\partial (\rho w)}{\partial t} + \frac{\partial (\rho uw)}{\partial x} + \frac{\partial (\rho vw)}{\partial y} + \frac{\partial (\rho w^2)}{\partial z} = \frac{\partial \rho}{\partial y} + \frac{1}{Re_r}\left(\frac{\partial \tau_{xz}}{\partial x} + \frac{\partial \tau_{yz}}{\partial y} + \frac{\partial \tau_{zz}}{\partial z}\right) \tag{7}$$

OpenFOAM numerical model solves the Navier-Stokes equation through the x, y, and z direction described in equations (4), (5), (6), and (7) where u, v, and w are the velocity components in the x, y, and z direction, ρ is density, t is the time, Re for Reynolds number, τ is a moment of force or torque.

3.0 RESULT AND DISCUSSION

3.1 Time Measurement of Mesh Computation

Flow velocity in channel junctions is a critical physical parameter that determines the formation of secondary flow patterns. The impact of channel geometry on water flow velocity has been analyzed through the velocity profile within depth. Figure 3 illustrates the velocity profiles for each variation angle of the channel junction, with the data points adjusted according to the geometry of the channel. Velocity data were taken precisely at the intersection where the main channel flow meets the branch channel flow. This area is characterized as the area with high velocity, known as the contraction zone.

Velocity data for the 90°, 70°, and 50° channels were collected at points X = -1.5 and Y = 0.5, where the results are shown in Figures 3(a), (b), and (c). As for the 30° channel, data were collected at X = -2.5 and Y = 0.5, and for the 10° channel, data were taken at X = -5.5 and Y = 0.5, with the velocity profiles for these channels depicted in Figures 3(d) and (e). The analysis of the velocity profiles shows that the flow experiences both increases and decreases as it approaches the surface. This phenomenon is called the "Velocity-Dip Phenomenon," where the maximum velocity occurs below the free surface, reducing velocity near the surface [24]. The decrease in velocity at the surface layer is due to atmospheric pressure affecting the channel flow. This pressure creates friction with the surface flow, thereby causing the flow to slow down. Consequently, the maximum velocity occurs below the surface, where disturbances do not influence the flow.

3.2 Flow Velocity Analysis within Depth

In this study, the primary flow moves through the main channel while the branch channel flow enters the main channel. Five simulations of water flow were conducted using CFD utilizing Open FOAM software. These five simulations were performed with different branch angles, specifically 90°, 70°, 50°, 30° and 10° channel junctions. The changes in angle affect the velocity and flow patterns, which are then analyzed. The changes in velocity occurring in the outer layer of the channel are analyzed by considering the position/zones where the flow reaches maximum and minimum velocities. Figure 4 shows the 3D simulation illustration of the five angle variations for a water depth Z = 0.296 m. The result reveals that each junction angle has different velocity changes, creating secondary flow zones around the channel.

Figure 4 was analyzed by inputting an average velocity value of 0.628 m/s, which has been plotted in the Inlet1 and Inlet2 regions. The simulation results show that changes in the angle affect both the velocity and stability of the flow rate around the channel junction. Separation zones can be observed in the low-velocity areas along the wall near the branch channel in the 90°, 70°, and 50° junctions, as shown in Figure 4(a), (b), and (c), while Figure 4(d) and (e) shown no contraction zone formation is evident in the 30° and 10 junctions. The findings in this study show the same flow pattern as the analytical findings based on experimental data show in Figure 1 [1].

JOMAse | Received: 19-September-2024 | Accepted: 30-November-2024 | [(68) 3: 106-117]
Published by International Society of Ocean, Mechanical and Aerospace Scientists and Engineers, www.isomase.org., ISSN: 2354-7065 & e-ISSN: 2527-6085

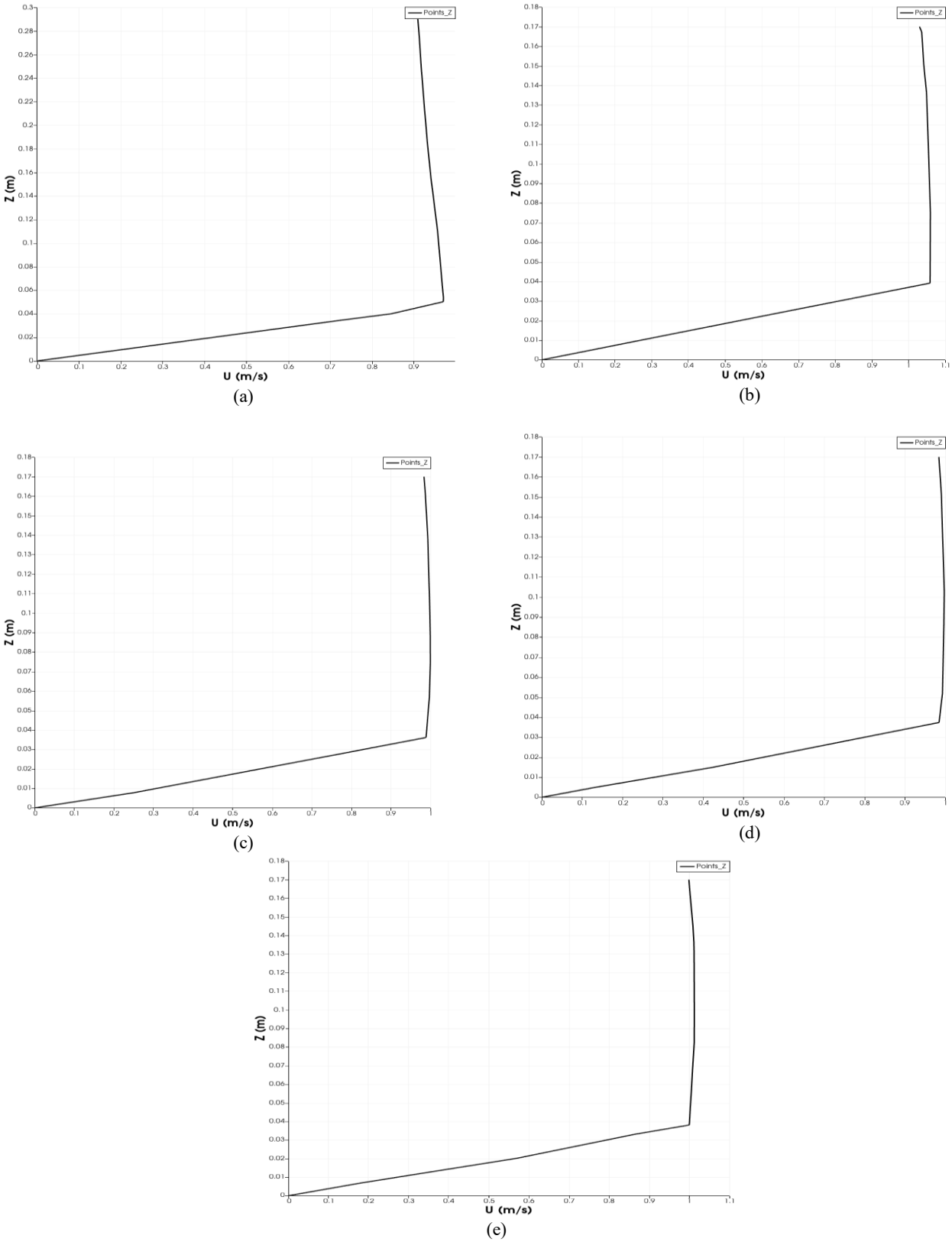

Figure 3: Velocity profile within depth near the confluence angle; (a) 90° channel junction, (b) 70° channel junction, (c) 50° channel junction, (d) 30° channel junction, and (e) 10° channel junction

JOMAse | Received: 19-September-2024 | Accepted: 30-November-2024 | [(68) 3: 106-117]
Published by International Society of Ocean, Mechanical and Aerospace Scientists and Engineers, www.isomase.org., ISSN: 2354-7065 & e-ISSN: 2527-6085

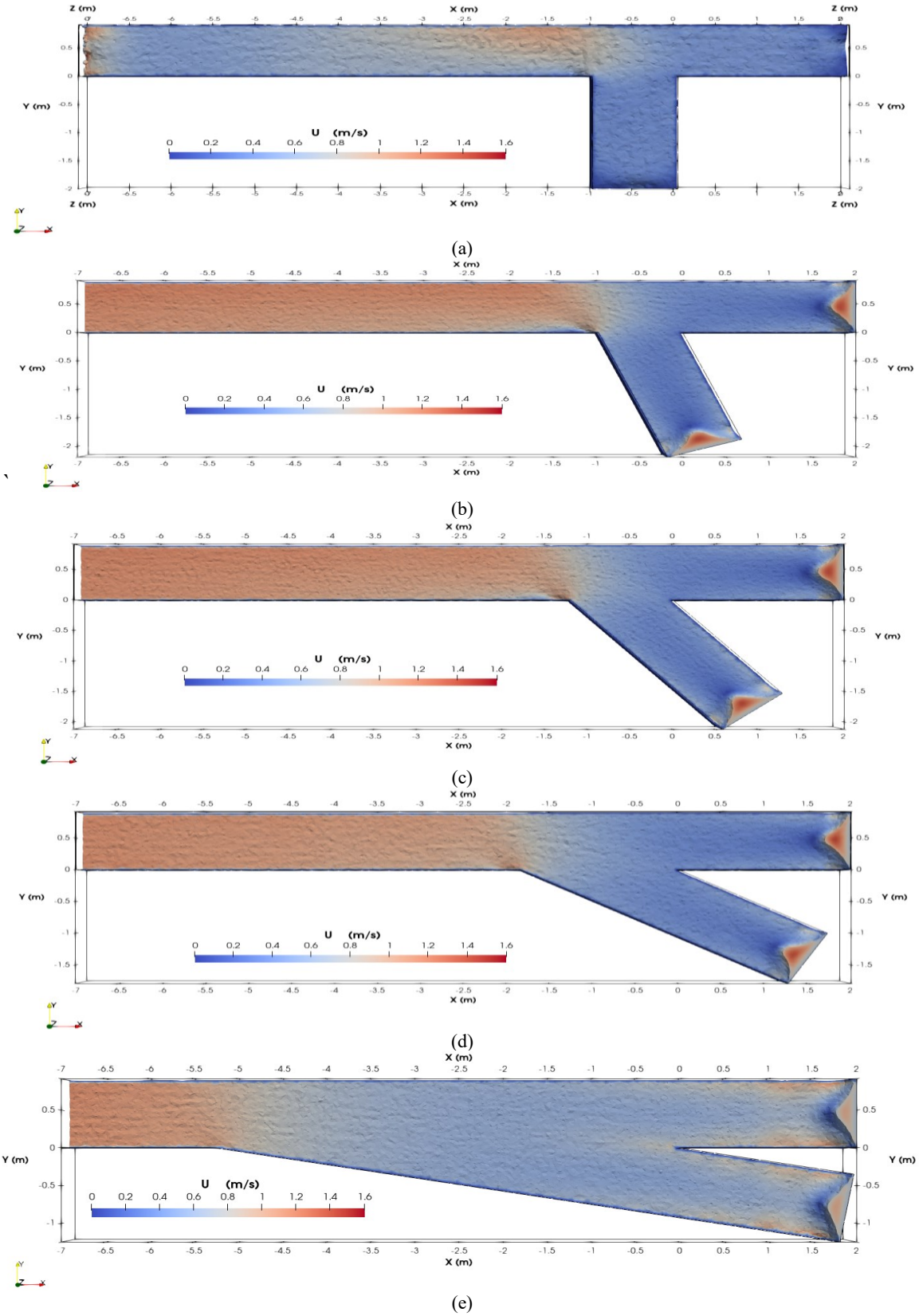

Figure 4: Simulation result of water flow in confluence channel where depth close to the surface at h = 0.296 m; (a) velocity distribution in 90° channel junction, (b) velocity distribution in 70° channel junction, (c) velocity distribution in 50° channel junction, (d) velocity distribution in 30° channel junction, and (e) velocity distribution in 10° channel junction

JOMAse | Received: 19-September-2024 | Accepted: 30-November-2024 | [(68) 3: 106-117]
Published by International Society of Ocean, Mechanical and Aerospace Scientists and Engineers, www.isomase.org., ISSN: 2354-7065 & e-ISSN: 2527-6085

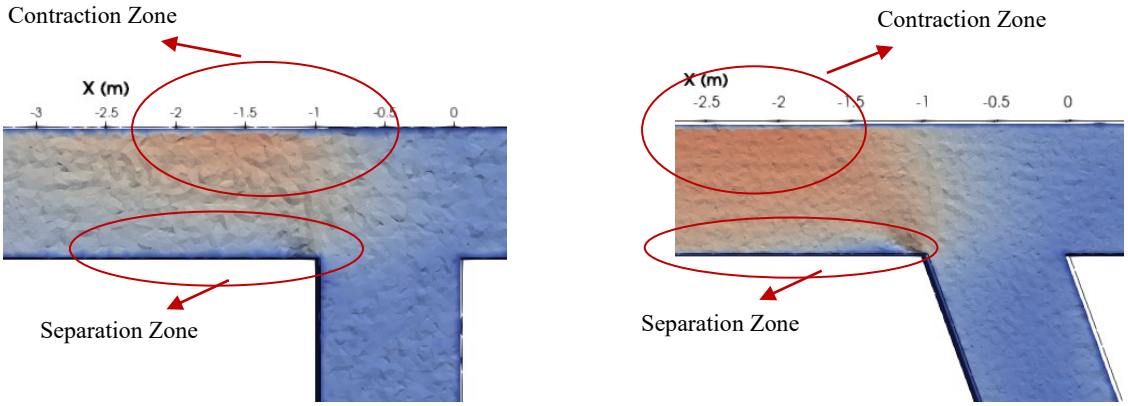

(a) (b)

Figure 5: Contraction and separation zone formed in confluent channel; (a) 90° channel junction, and (b) 70° channel junction

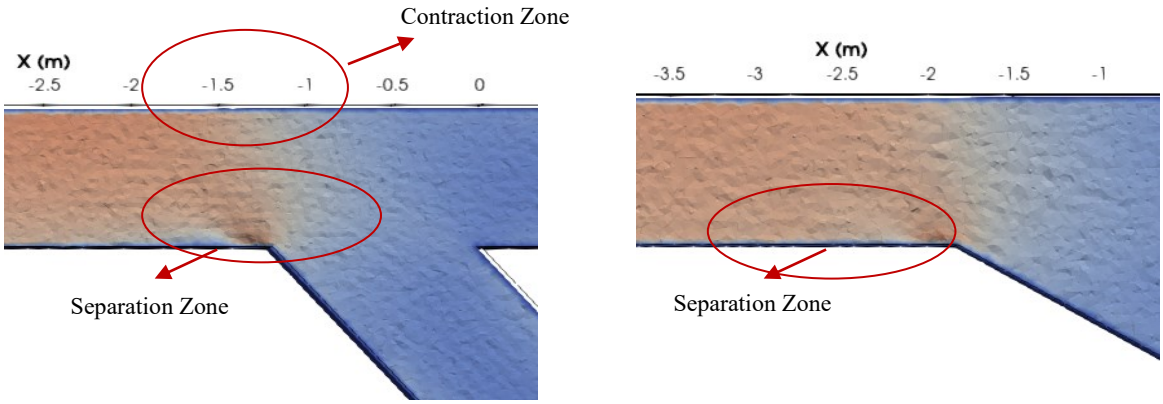

(a) (b)

Figure 6: Contraction and separation zone formed in confluent channel; (a) 50° channel junction, and (b) 30° channel junction.

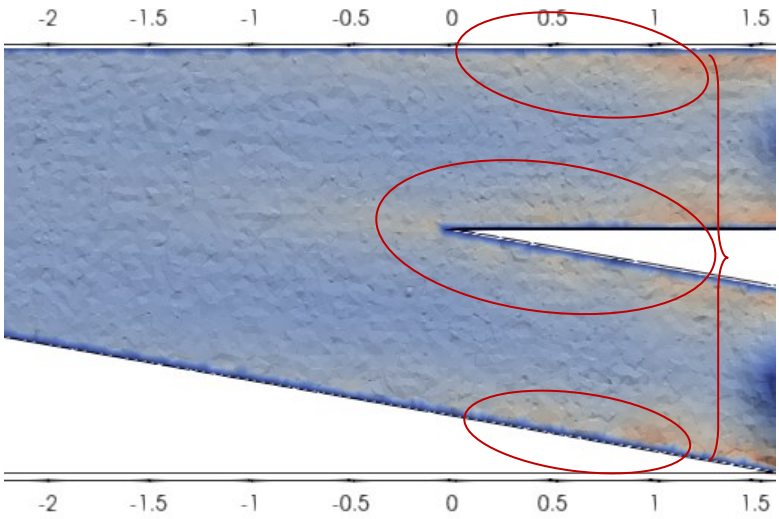

Zone with high velocity formed in channel caused by asymmetrical geometry

Figure 7: Velocity changes in channel wall at 10° channel junction

JOMAse | Received: 19-September-2024 | Accepted: 30-November-2024 | [(68) 3: 106-117]
Published by International Society of Ocean, Mechanical and Aerospace Scientists and Engineers, www.isomase.org., ISSN: 2354-7065 & e-ISSN: 2527-6085

Separation zones in the 90° and 70° channels form around the main channel wall area, as shown in Figure 5(a) and (b). This zone formed due to the velocity changes when the branch channel flow meets the main channel flow. The secondary flow patterns observed in the 90° and 70° channels are consistent with the confluent flow patterns shown in Figure 1, though with the differences in the areas of the zones formed. The contraction zone in the 70° channel is larger compared to the 90° channel, while the separation zone in the 90° channel is broader compared to the 70° channel. In contrast, Figure 6(a) shows that the 50° channel exhibits the same pattern as the 70° channel, where the separation zone area is slightly the same and located near the junction in the inner bank of the main channel. The velocity in the main channel flow reaches its maximum when meeting the branch channel flow, forming a low-pressure zone around the inner bank. Misalignment in the geometry can cause the displacement of this zone. Similarly, the 30° and 10° channels show no significant changes in velocity within the main channel. Figure 6 (b) illustrates that in the 30° channels; the flow velocity is relatively stable, showing no significant reduction in velocity flow. In contrast, Figure 7 shows that the 10° channel exhibits a different pattern, where the separation zone is located around the branch channel due to the asymmetric channel geometry. In cases of asymmetric flow confluence, separation zones typically form in the tributary channel due to the linear shape of the main channel [25]. Thus, the 10° channel reaches its maximum velocity around the main channel's inner bank, forming a separation zone in the branch channel. In practical applications in rivers, this zone can trigger riverbank degradation.

The channel bed is generally the area with the lowest velocity. However, the confluences of flows between two channels may cause this region's velocity changes. Therefore, an analysis was also conducted on the channel bed area to examine the potential impact of frictional forces on water flow and velocity changes. Paraview was used to slice and visualize the simulation area at a depth of Z = 0.05 m near the channel bed, as shown in Figure 8. The results indicate that the flow at a depth of Z = 0.05 m near the channel bed is not significantly different from the flow pattern at a depth of Z = 0.296 m due to the relatively small difference in depth. Figure 8(a) presents the flow visualization at a Z = 0.05 m depth in the 90° channel. It is observed that the separation zone formed at a depth of Z = 0.296 m due to the velocity reduction, which also extends to a depth of Z = 0.05 m. The interaction between the frictional forces and the channel bed causes the velocity to decrease with increasing depth. Similarly, changes in velocity and the formation of low and high-velocity zones are also observed in the 70°, 50°, 30°, and 10° channels, as shown in Figures 8(b), (c), (d), and (e), with results of velocity and flow pattern not significantly differing from those at a depth of Z = 0.296 m. Understanding the regions where velocity changes occur is crucial for predicting areas with a higher likelihood of sediment deposition, as trapped particles will settle or accumulate at the channel bed.

3.3 Vector Analysis

Vector fields can illustrate the velocity direction by utilizing the results from OpenFOAM through ParaView software. Figure 9 shows the processed velocity data in vector format, where the flow direction at this layer was interpreted for the five angle variations. The vector analysis reveals that the flow patterns at different angles remain relatively stable, with differences in the area of the patterns formed by the changes in velocity. Based on the vector analysis, several points in the channel exhibit a reduction in velocity, such as at the inner bank around the main channel in the 90°, 70°, and 50° channels, as shown in Figures 9(a), (b), and (c), which also shown the potential for sediment or other particles to trapped in these regions. The vector results in Figure 9(d) indicate that the velocity of the flow when the main flow meets the branch flow is relatively stable and does not form unusual patterns.

However, several points around the branch channel show an increase in velocity due to the flow impact in the asymmetric channel at the 10° channel, as illustrated in Figure 9(d). The velocity vector analysis was conducted at a depth of Z = 0.296 m, focusing on the flow direction towards the negative x-axis while considering its motion direction. Figure 10 shows that the confluences of flows create a zone where the flow direction changes or deflects. In this zone, the main channel flow will bend to follow the branch channel's flow, resulting in a secondary flow in the recovery zone around the outer bank. The junction angle and geometry play a crucial role in enhancing the turbulence and secondary flow distribution, which also affects the morphology of the confluence area [15]. An increased water flow velocity generally characterizes this zone, whereas the separation zone is marked by decreased velocity around the channel. In river applications, this zone is typically where sedimentation is trapped and settles. Meanwhile, the stagnation zone is characterized by a flow with zero velocity.

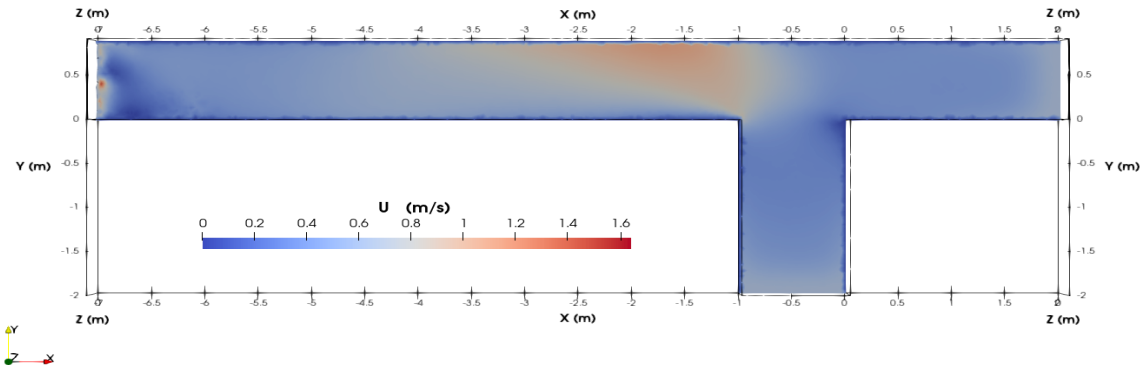

(a)

JOMAse | Received: 19-September-2024 | Accepted: 30-November-2024 | [(68) 3: 106-117]
Published by International Society of Ocean, Mechanical and Aerospace Scientists and Engineers, www.isomase.org., ISSN: 2354-7065 & e-ISSN: 2527-6085

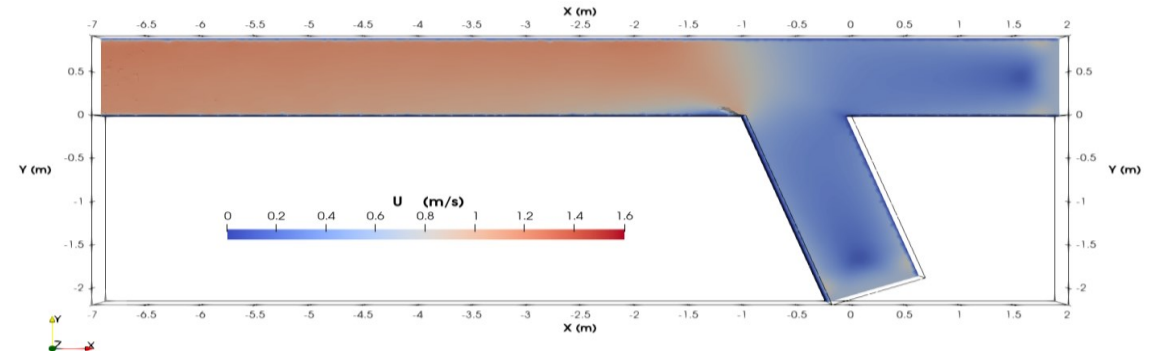

(b)

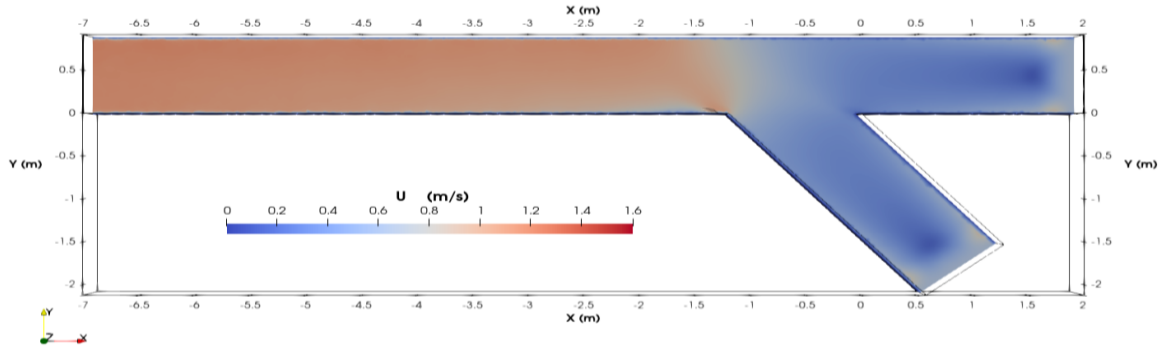

(c)

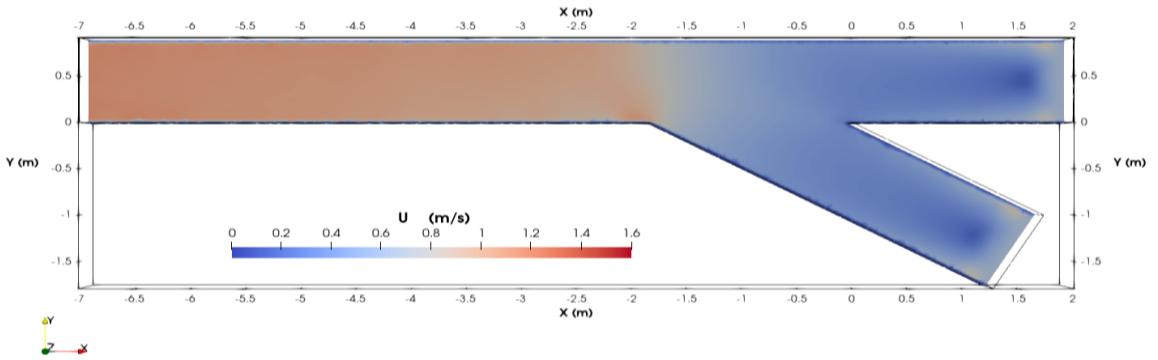

(d)

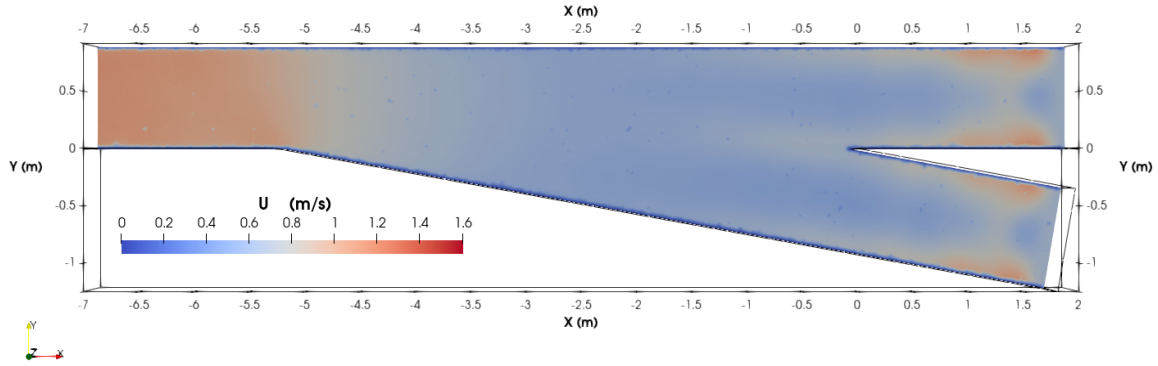

(e)

Figure 8: Simulation result of water flow in confluence channel where depth close to the bed at h = 0.05 m; (a) velocity distribution in 90° channel junction, (b) velocity distribution in 70° channel junction, (c) velocity distribution in 50° channel junction, (d) velocity distribution in 30° channel junction, and (e) velocity distribution in 10° channel junction.

JOMAse | Received: 19-September-2024 | Accepted: 30-November-2024 | [(68) 3: 106-117]
Published by International Society of Ocean, Mechanical and Aerospace Scientists and Engineers, www.isomase.org., ISSN: 2354-7065 & e-ISSN: 2527-6085

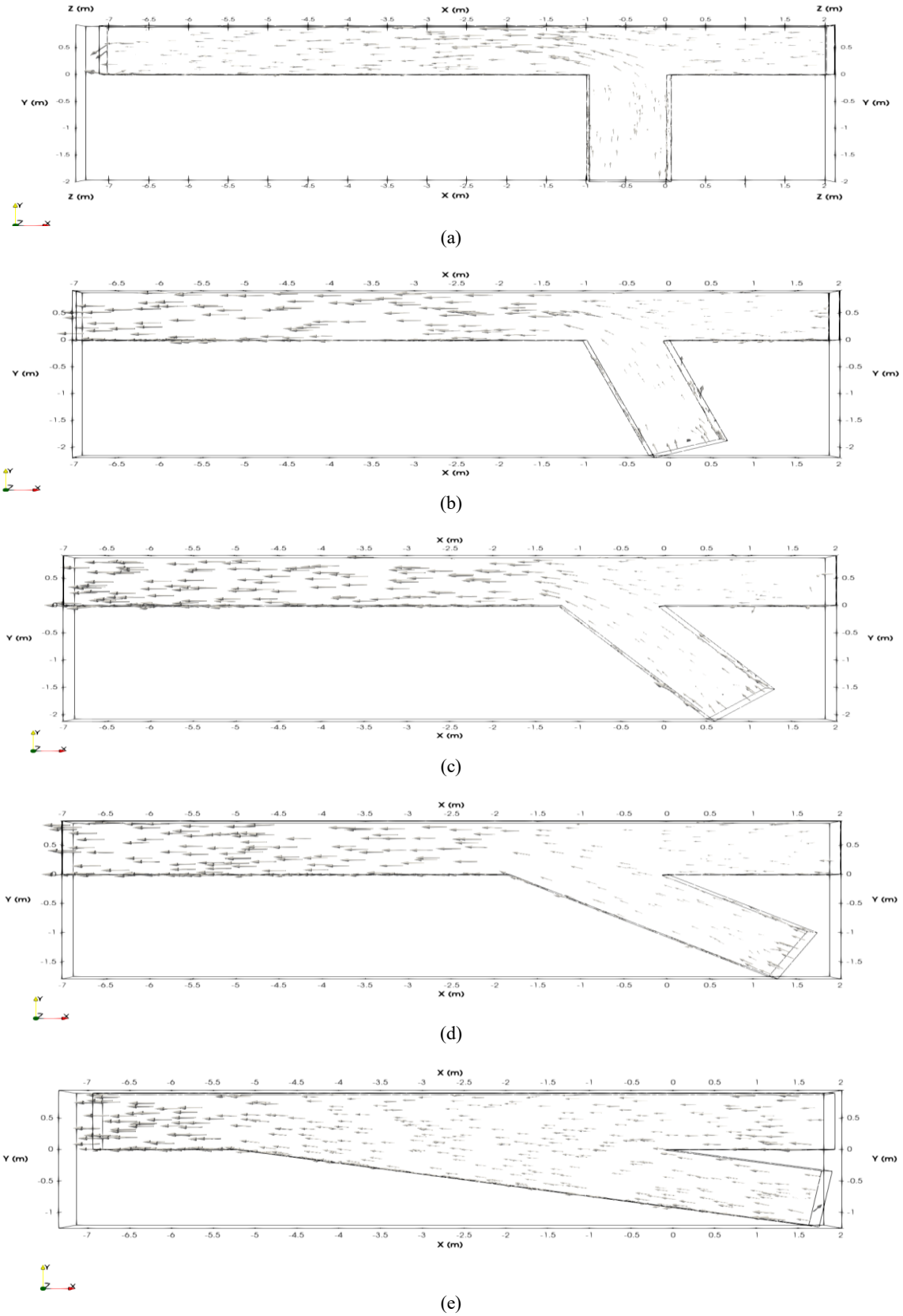

Figure 9: Vector view in confluence channel based on velocity; (a) 90° channel junction, (b) 70° channel junction, (c) 50° channel junction, (d) 30° channel junction, and (e) 10° channel junction

JOMAse | Received: 19-September-2024 | Accepted: 30-November-2024 | [(68) 3: 106-117]
Published by International Society of Ocean, Mechanical and Aerospace Scientists and Engineers, www.isomase.org., ISSN: 2354-7065 & e-ISSN: 2527-6085

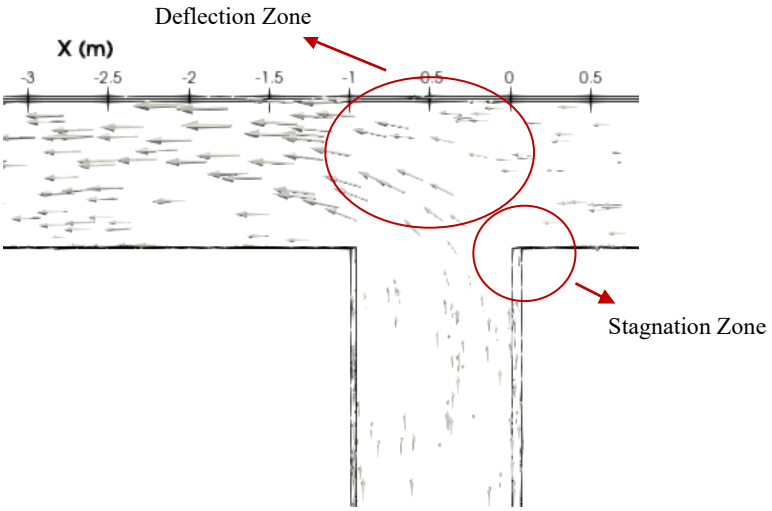

Figure 10: Vector analysis around the 90° channel junction

4.0 CONCLUSION

This study successfully met the initial objective to investigate the effects of secondary flow at the confluence of two open channels with various angle variations using a Computational Fluid Dynamics (CFD) approach. Simulations performed with OpenFOAM software showed that variations in the confluence angle (90°, 70°, 50°, 30°, and 10°) significantly affected the flow velocity and the formation of secondary flow zones, including contraction, separation, stagnation, and deflection zones. These results confirm that the angle variation affects the flow dynamics and energy distribution in the confluence area, which can be used to improve transportation safety in this area, optimize shipping routes, and predict sediment deposition areas. This study provides a solid foundation for further development, including the use of alternative turbulence models and the investigation of the influence of obstacles for sedimentation management purposes.

ACKNOWLEDGEMENTS

The authors would like to thank the educator in the Faculty of Mathematics and Natural Science, Tanjungpura University, for significantly contributing to the refinement and enhancement of this research.

REFERENCES

[1] Shaheed, R., Yan, X. & Mohammadian, A. (2021). Review and comparison of numerical simulations of secondary flow in river confluences. *Water*, *13*(14), 1917.

[2] Constantinescu, G., Koken, M. & Zeng, J. (2010). Simulation of flow in an open channel bend of strong curvature using Detached Eddy Simulation. In *River Flow* (Vol. 2010, pp. 1527-1534). Karlsruhe, Germany: Bundesanstalt Für Wasserbau.

[3] Bilal, A., Xie, Q. & Zhai, Y. (2020). Flow, sediment, and morpho-dynamics of river confluence in tidal and non-tidal environments. *Journal of Marine Science and Engineering*, *8*(8), 591.

[4] Shakibainia, A., Tabatabai, M.R.M. & Zarrati, A.R. (2010). Three-dimensional numerical study of flow structure in channel confluences. *Canadian Journal of Civil Engineering*, *37*(5), 772-781.

[5] Putra, Y.S., Noviani, E., Kurnia, E. & Christy, M.C.P. (2024). Numerical analysis of sedimentation in open channels using computational fluid dynamics. *Journal of Ocean, Mechanical and Aerospace*, 66(2), 53-63.

[6] Nazari-Giglou, A., Jabbari-Sahebari, A., Shakibaeinia, A. & Borghei, S.M. (2016). An experimental study of sediment transport in channel confluences. *International Journal of Sediment Research*, *31*(1), 87-96.

[7] Shumate, E.D. (1998). Experimental Description of Flow at an Open Channel Junction; University of Iowa: Iowa City, IA, USA.

[8] Yang, Q.Y., Liu, T.H., Lu, W.Z. & Wang, X.K. (2013). Numerical simulation of confluence flow in open channel with dynamic meshes techniques. *Advances in Mechanical Engineering*, *5*, 860431.

[9] Birjukova, O., Ludena, S., Alegria, F. & Cardoso, A. (2014). Three-dimensional flow field at confluent fixed-bed open channels. *River Flow 2014- Schleiss et al. (Eds)*, 1007-1014.

[10] Versteeg, H.K. & Malalasekera, W. (2007). An Introduction to Computational Fluid Dynamics: The Finite Volume Method, Pearson Education Limited.

[11] Mahananda, M. & Hanmaiahgari, P. R. (2018). Effect of aspect ratio on higher order moments of velocity fluctuations in hydraulically rough open channel flow. In *E3S Web of Conferences* (Vol. 40, p. 05045). EDP Sciences.

[12] Akbari, M. & Vaghefi, M. (2017). Experimental investigation on streamlines in a 180º sharp bend. *Acta Scientiarum. Technology*, *39*(4), 425-432.

[13] Shaheed, R., Mohammadian, A. & Yan, X. (2021). A review of numerical simulations of secondary flows in

JOMAse | Received: 19-September-2024 | Accepted: 30-November-2024 | [(68) 3: 106-117]
Published by International Society of Ocean, Mechanical and Aerospace Scientists and Engineers, www.isomase.org., ISSN: 2354-7065 & e-ISSN: 2527-6085

river bends. *Water*, *13*(7), 884.
[14] Shaheed, R., Yan, X. & Mohammadian, A. (2021). Review and comparison of numerical simulations of secondary flow in river confluences. *Water*, *13*(14), 1917.
[15] Binesh, N. & Bonakdari, H. (2014). Longitudinal velocity distribution in compound open channels: comparison of different mathematical models. *International Research Journal Application Basic Science*, *8*, 1149-1157.
[16] Russell, P. & Vennell, R. (2019). High resolution observations of an outer-bank cell of secondary circulation in a natural river bend. *Journal of Hydraulic Engineering*, *145*(5), 04019012.
[17] Shaheed, R., Mohammadian, A. & Kheirkhah Gildeh, H. (2019). A comparison of standard k–ε and realizable k–ε turbulence models in curved and confluent channels. *Environmental Fluid Mechanics*, *19*, 543-568.
[18] Kheirkhah Gildeh, H., Mohammadian, A., Nistor, I. & Qiblawey, H. (2015). Numerical modeling of 30^0 and 45^0 inclined dense turbulent jets in stationary ambient. *Environmental Fluid Mechanics*, *15*, 537-562.
[19] Talebpour, M. (2016). Numerical Investigation of Turbulent-Driven Secondary Flow. M.Sc. thesis, Pennsylvania State Univ.
[20] Gholami, A., Akhtari, A.A., Minatour, Y., Bonakdari, H. & Javadi, A.A. (2014). Experimental and numerical study on velocity fields and water surface profile in a strongly-curved 90^0 open channel bend. *Engineering Applied Computing Fluid Mechanic* 8, 447-461.
[21] Ludeña S. G. (2015). Hydro-Morphodynamics of Open-Channel Confluences with Low Discharge Ratio and Dominant Tributary Sediment Supply. PhD thesis, Department of Civil Engineering, Architecture, and Georesources, University of Lisbon, Portugal.
[22] Riesterer, J., Wenka, T., Brudy-Zippelius, T. & Nestmann, F. (2016). Bed load transport modeling of a secondary flow influenced curved channel with 2D and 3D numerical models. *Journal of Applied Water Engineering and Research*, *4*(1), 54-66.
[23] Holzinger, G. (2015). OpenFOAM a little user-manual. *CD-Laboratory-Particulate Flow Modelling, Johannes Keplper University: Linz, Austria*.
[24] Vanoni, V. A. (1941). Velocity distribution in open channels. *California Institute of Technology, Reprinted from: Civil Engineering:ASCE* 11(6), 356-357.
[25] Biron, P., Best, J. L., & Roy, A. G. (1996). Effects of bed discordance on flow dynamics at open channel confluences. *Journal of Hydraulic Engineering*, *122*(12), 676-682.

JOMAse | Received: 19-September-2024 | Accepted: 30-November-2024 | [(68) 3: 106-117]
Published by International Society of Ocean, Mechanical and Aerospace Scientists and Engineers, www.isomase.org., ISSN: 2354-7065 & e-ISSN: 2527-6085